Exploring hydro-meteorological drought patterns over the Greater Horn of Africa (1979-2014) using remote sensing and reanalysis products

Advances in Water Resources, 2016

Exploring hydro-meteorological drought patterns over the Greater Horn of Africa (1979-2014) using remote sensing and reanalysis products

J.L. Awange[a,b,c], Khandu[a], M. Schumacher[d], E. Forootan[a,d,e], B. Heck[b]

[a] *Western Australian Centre for Geodesy and The Institute for Geoscience Research Curtin University, Perth, Australia*
[b] *Geodetic Institute, Karlsruhe Institute of Technology, Karlsruhe Germany*
[c] *Department of Geophysics, Kyoto University, Japan*
[d] *Institute of Geodesy and Geoinformation, Bonn University, Bonn, Germany*
[e] *School of Earth and Ocean Sciences, Cardiff University, Cardiff, UK*

Abstract

Spatio-temporal patterns of hydrological droughts over the Greater Horn of Africa (GHA) are explored based on total water storage (TWS) changes derived from time-variable gravity field solutions of Gravity Recovery and Climate Experiment (GRACE, 2002-2014), together with those simulated by Modern Retrospective Analysis for Research Application (MERRA, 1980-2014). These hydrological extremes are then related to meteorological drought events estimated from observed monthly precipitation products of Global Precipitation Climatology Center (GPCC, 1979-2010) and Tropical Rainfall Measuring Mission (TRMM, 1998-2014). The major focus of this contribution lies on the application of spatial Independent Component Analysis (sICA) to extract distinguished regions with similar rainfall and TWS with similar overall trend and seasonality. Rainfall and TWS are used to esti-

Email address: schumacher@geod.uni-bonn.de (M. Schumacher)

mate Standard Precipitation Indices (SPIs) and Total Storage Deficit Indices (TSDIs) respectively that are employed to characterize frequency and intensity of hydro-meteorological droughts over GHA. Significant positive (negative) changes in monthly rainfall over Ethiopia (Sudan) between 2002 and 2010 leading to a significant increase in TWS over the central GHA region were noted in both MERRA and GRACE TWS (2002-2014). However, these trends were completely reversed in the long-term (1980-2010) records of rainfall (GPCC) and TWS (MERRA). The four independent hydrological sub-regions extracted based on the sICA (i.e., Lake Victoria Basin, Ethiopia-Sudanese border, South Sudan, and Tanzania) indicated fairly distinct temporal patterns that matched reasonably well between precipitation and TWS changes. While meteorological droughts were found to be consistent with most previous studies in all sub-regions, their impacts are clearly observed in the TWS changes resulting in multiple years of extreme hydrological droughts. Correlations between SPI and TSDI were found to be significant over Lake Victoria Basin, South Sudan, and Tanzania. The low correlations between SPI and TSDI over Ethiopia may be related to inconsistency between TWS and precipitation signals. Further, we found that hydrological droughts in these regions were significantly associated with Indian Ocean Dipole (IOD) events with El Niño Southern Oscillation (ENSO) playing a secondary role.

Keywords: Greater Horn of Africa, Total Storage Deficit Index (TSDI), Standardized Precipitation Index (SPI), spatial Independent Component Analysis (sICA), ENSO, IOD

---

1. Introduction

The people of the semi-arid region of Greater Horn of Africa (GHA) largely depend on rain-fed agriculture and livestock that is increasingly coming under threat from the intensified frequency and severity of drought events over the past decades (e.g., Kurnik et al., 2011). Since most crops in GHA are planted during rainy seasons, i.e., March-May (MAM) and October-December (OND), food security is increasingly coming under jeopardy given the fact that these seasons too are now reported to experience drought episodes (Marthews et al., 2015). This is further exacerbated by the continued warming of the Indian-Pacific Oceans possibly linked to anthropogenic influences or multi-decadal climate variability, which has been shown to contribute to more frequent droughts in GHA over the past 30 years during the spring and summer seasons (see, e.g., Williams & Funk, 2011; Lyon, 2014; Funk et al., 2014).

Even with the reality of the threat posed by droughts in the GHA, see e.g., Lyon (2014), effective drought monitoring in this region is, however, challenged by multiple factors including: inadequate spatial coverage and hydro-meteorological observations (e.g., precipitation, temperature, soil moisture, and groundwater storage) that are not readily available beyond the local meteorological services, poor communication frameworks, and national red tapes in accessing data.

Furthermore, the large spatial extent of GHA makes the collection of hydrological data quite challenging and hence the reason why most studies (e.g., Viste et al., 2013) have focused largely on meteorological droughts. This view is supported e.g., by Naumann et al. (2014) who pointed out that the

lack of reliable hydro-meteorological data hold up development of effective real-time drought monitoring and early warning systems in the region. To account for various drought conditions over GHA, therefore, an integrated drought index that involves various meteorological and hydrological variables is desirable (e.g., the African Drought Monitor (ADM[1]) project; Sheffield et al., 2014). This, therefore, highlights the significant role played by satellite remote sensing in data deficient regions.

To this extent, the Gravity Recovery and Climate Experiment (GRACE, Tapley et al., 2004) satellite remote sensing mission, launched in 2002, offers the possibility to characterize droughts at a wider spatial coverage albeit for shorter time span (from 2002 onwards). The value of GRACE-derived total water storage (TWS) changes for drought sutdies and estimating e.g., a Total Storage Deficient Index (TSDI), has been demonstrated (e.g., in Andersen et al., 2005; Yirdaw et al., 2008; Agboma et al., 2009; Leblanc et al., 2009; Chen et al., 2009, 2010; Houborg et al., 2012; Long et al., 2013; Li & Rodell, 2014; Thomas et al., 2014).

Although GRACE has the capability to offer a wider spatial coverage, spatio-temporal analysis of drought in GHA using a single areal-average as a representation of the entire GHA region is challenging. This is mainly due to the meteorological observations that are influenced by spatial inhomogeneity of climate over the GHA caused by uneven topography, north-south migration of Inter-tropical Convergence Zone (ITCZ), and spatially varying influences of large-scale climate events among others (see e.g., Viste et al.,

[1]http://stream.princeton.edu/AWCM/WEBPAGE/interface.php?locale=en

2013).

In this contribution, as opposed to Awange et al. (2008), Awange et al. (2013), Awange et al. (2014a) and Awange et al. (2014b) that focused mainly on TWS changes in Lake Victoria Basin, Nile Basin and Ethiopia, GRACE satellites and sICA method (Forootan & Kusche, 2012, 2013; Forootan et al., 2012) are employed for the first time to characterize meteorological and hydrological droughts in the entire GHA. The novelty is that for the first time, the long-term (1980-2014) meteorological and hydrological drought in GHA is extracted usind the Standardized Precipitation Index (SPI) and TSDI, respectively. The spatio-temporal variability of SPI and ISDI is also compared and a comprehensive interpretation of various drought events across the GHA is provided.

Specifically, the study (i) applies sICA to partition the GHA into various sub-regions based on precipitation and TWS changes, (ii) employs GRACE (2002-2014) and Modern Retrospective Analysis for Research Application (MERRA, 1980-2014) TWS changes to derive hydrological drought indices for the four independent sub-regions (as computed in i), (iii) uses observed precipitation products, Global Precipitation Climatology Center (GPCC, 1979-2010) and Tropical Rainfall Measuring Mission (TRMM, 1998-2014) to compute remotely sensed SPI, and (iv) examines the relative influence of ENSO and IOD events on hydro-meteorological droughts (reflected in TSDI and SPI) within the GHA sub-regions.

The remainder of the study is organized as follows. In section 2, a general climatological background of GHA is presented while section 3 presents an overview of the data as well as the analysis methods used. In section 4, the

drought indicators used in this study are described, while in section 5, the results are analysed and interpreted. The study is concluded in section 6.

2. Greater Horn of Africa (GHA): Climatological Background

The GHA, a semi-arid region, is made up of Burundi, Djibouti, Ethiopia, Eritrea, Kenya, Rwanda, Somalia, South Sudan, Sudan, Tanzania and Uganda. Long rains over equatorial GHA region mostly occur during March-May (MAM, Figure 1b) while short rains occur in October-December (OND, Figure 1d) corresponding to the migration of the intertropical convergence zone (ITCZ) from south to north and vice versa (Marthews et al., 2015). Furthermore, Ethiopia, South Sudan, Sudan, and parts of Uganda experience a single rainy season from June-September (JJAS) Figure 1c).

Apart from its seasonal differences, rainfall variability over the GHA is closely associated with the large-scale regional and global circulations such as ENSO, fluctuation of the Indian Ocean and Atlantic Ocean SST, and moisture fluxes over the Congo region (e.g., Nicholson, 1997; Williams et al., 2012; Tierney et al., 2013; Lyon, 2014). Mean temperature patterns over GHA follow the annual rainfall pattern.

3. Data

The data used in this study include monthly precipitation products obtained from global gridded rain gauge and near-global satellite-based estimates, as well as TWS changes from a reanalysis model and GRACE time-variable gravity field solutions.

3.1. Precipitation Products

1. *GPCC v6*: The Global Precipitation Climatology Center (GPCC) provides gridded precipitation products at various temporal and spatial resolutions derived from up to 67,000 quality controlled station data around the world between 1901 and 2010 (Schneider et al., 2014). This study used monthly precipitation data at 0.50° × 0.50° (latitude × longitude) spatial resolution covering the period 1979-2010. GPCC products have been found to be consistent with other rainfall products in Africa (see e.g., Awange et al., 2015). The distribution of rain gauges over the GHA region, however, is rather sparse over certain areas such as Somalia, Sudan, and Tanzania, and as such may not provide accurate representation of the precipitation variability over these regions.
2. *TRMM 3B43*: To complement the GPCC v6 data for the most recent period, monthly precipitation estimates from the Tropical Rainfall Measuring Mission (TRMM) Multi-satellite Precipitation Analysis (TMPA, Huffman et al., 2007) version 7 for the period 1998 to 2014 were used. These products at 0.25° × 0.25° spatial resolution were interpolated to 0.50° × 0.50° to make them consistent with those of GPCC. Awange et al. (2015) assessed various precipitation products over Africa covering 2003-2010, from which TRMM 3B43 (hence forth referred to as TRMM) indicated similar skills compared to GPCC v6.

[FIGURE 1 AROUND HERE.]

3.2. GRACE Level-2 Data

In this study, the reprocessed GRACE Level-2 RL05a time-series for the period 2002 to 2014 from the Gravity Recovery and Climate Experiment

(GRACE, e.g., Tapley et al., 2004) was used. The GRACE data is provided by GeoForschungsZentrum (GFZ, Potsdam, Dahle et al., 2013) as sets of (approximately) monthly fully normalized geopotential spherical harmonic coefficients up to degree and order 90 (see, ftp://podaac.jpl.nasa.gov/allData/grace/L2/).

GRACE degree one (C_{10}, C_{11}, S_{10}) coefficients were replaced by those from Cheng et al. (2013), and the more accurate degree two coefficients derived from satellite laser ranging (SLR, Cheng & Tapley, 2004) replaced C_{20}. A commonly used non-isotropic de-correlation filter (DDK3, Kusche et al., 2009; Forootan, 2014) was applied to reduce the high degree/order correlated errors, which are manifested as stripes in the spatial domain. This filter removes most of north-south stripes and seems to be suitable to process GFZ RL05a products over the GHA. To be consistent with GPCC, the time-variable spherical harmonic coefficients were converted to $0.50^\circ \times 0.50^\circ$ (latitude $\times$ longitude) TWS grids using the approach of Wahr et al. (1998). The selected spatial grid is optimistic for GRACE products whose spatial resolution is $\sim 1^\circ$.

3.3. MERRA Data

GRACE TWS estimates were compared with those simulated by the Modern Retrospective Analysis for Research Application (MERRA, Rienecker et al., 2011). MERRA reanalysis are run globally at a relatively high spatial resolution ($0.67^\circ \times 0.50^\circ$) and are available as monthly products from 1979-present. In this study, monthly MERRA-LAND TWS estimates for the period 1980 to 2014 were processed by filtering in the spectral domain and then converted to a grid resolution of $0.50^\circ \times 0.50^\circ$ to be consistent with

those of GRACE and GPCC products.

Filtering of both GRACE and MERRA products, however, causes some damping of the signal amplitude and might introduce spatial leakages, which should be restored by introducing a multiplicative scaler (or a gridded) gain factor (e.g., Landerer & Swenson, 2012). A multiplicative scale factor of 1.05 was obtained from the MERRA TWS and was uniformly applied to both GRACE and reanalysis data used in this study.

4. Hydro-meteorological Drought Indices

To assess the hydro-meteorological drought events, two drought indicators were analysed: (i) the Standard Precipitation Index (SPI) estimated from monthly precipitation products of GPCC and TRMM, and (ii) the Total Storage Deficit Index (TSDI) deduced from MERRA and GRACE. Drought conditions were assessed over various sub-regions of the GHA extracted using the spatial independent component analysis approach discussed in Section 4.3.

4.1. Standardized Precipitation Index (SPI)

The Standardized Precipitation Index (SPI) is a widely-used meteorological drought indicator based on probability distribution of long-term rainfall time-series developed by McKee et al. (1993, 1995) to provide a spatially and temporally invariant measure of rainfall deficit (or excess) over a variety of accumulation timescales (e.g., 3, 6, 12, 24 months). SPI is derived by fitting a parametric cumulative probability distribution (CDF) of e.g., γ-distribution to the precipitation time-series, which are then transformed to obtain the SPI using the inverse normal (Gaussian) distribution function (e.g., Viste

et al., 2013). SPI provides the value of standard anomalies from the median indicating negative for drought and positive for wet conditions (see details in Table 1). In this study, SPI is computed for the 12-month accumulation time periods to capture the long-term trend of meteorological droughts over the GHA.

[TABLE 1 AROUND HERE.]

4.2. Total Storage Deficit Index (TSDI)

The Total Storage Deficit Index (TSDI) is a renamed version of Soil Moisture Deficient Index (SMDI, Narasimhan & Srinivasan, 2005) by Yirdaw et al. (2008). TWS changes, which comprise information of the changes in all water components (surface, groundwater, soil moisture, biomass, ice and snow) are used in this study to compute TSDI. The procedure to estimate TSDI (based on GRACE data) involves an estimation of the Total Storage Deficit as (TSD%, Yirdaw et al., 2008):

$$TSD(k, j-2001) = \frac{TWS(k,j) - Mean(TWS(k,:))}{Max(TWS(k,:)) - Min(TWS(k,:))} \times 100, \qquad (1)$$
$$k = 1, 2, \ldots, 12, j = 2002, 2003, \ldots, 2014$$

where $TWS(k,j)$ is the k'th month of total water storage (anomaly) in each year ($j = 2002, 2003, \ldots, 2014$) obtained from GRACE. For MERRA, the left hand side of Eq. 1 becomes $TSD(k, j-1979)$ and $j = 1980, 1981, \ldots, 2014$. $Mean(TWS(k,:))$, $Max(TWS(k,:))$, and $Min(TWS(k,:))$ are respectively the mean, maximum, and minimum of the k'th month of TWS over the study period (for GRACE covering 2002-2014 and for MERRA 1980-2014).

The TSD values in Eq. 1 can be stored in a vector TSD_i ($i = 1, 2, \ldots,$ length of TWS time series). Consequently, TSDI can be computed as

$$TSDI_i = p \times TSDI_{i-1} + q \times TSD_i, \tag{2}$$

where the drought severity and duration factors p and q are defined from the cumulative TSD plot (e.g., Figure 2) based on the following relation (Yirdaw et al., 2008):

$$p = 1 - \frac{m}{m+b}, \qquad q = -\frac{C}{m+b}. \tag{3}$$

In Eq. 3, C represents drought intensity, which is obtained from the best fit line of the cumulative TSD (from the drought monograph) during the dryness period (see e.g., line 3 in Figure 2). In general, C can take on any of the four drought classifications values (-4.0 for extreme drought, -3.0 for severe drought, -2.0 for moderate drought, and -1.0 for mild drought) defined according to Palmer (1965). The other elements of the regression line are the slope m and the intercept b of the best fit of the drought monograph for the dryness period of the cumulative TSD curve.

Using an example, we illustrate how the TSDI values of this study are estimated. Figure 2(a) shows a TSD (%) plot over Ethiopia derived from GRACE TWS changes based on Eq. 1 between 2004 and 2013. A prolonged drought pattern from March 2004 to November 2006 (33 months) has been detected with the TSD values reaching as low as 66%. Assuming this scenario, we plot the cumulative TSDs in Figure 2(b) to derive the parameters in Eqs. 2-3. Using the linear regression parameters during the declining TWS period (i.e., 2004-2007), TSDI was computed for the period of decline.

The slope ($m = -31.54$) and y-intercept ($b = -20.51$) parameters derived from the cumulative TSD based on 33 months from March 2004 to November 2006 were subsequently used to calculate the critical parameters p and q. Therefore, C= -3 is the category of drought event as can be seen in Figure 2. Correspondingly p and q were derived as 0.394 and 0.058, respectively. $TSDI_{1,1}$ was assumed to be 2% of TSD_1 in line with Yirdaw et al. (2008). The TWS droughts, categorized based on the "C" values of Figure 2, are reported in Table 2. This procedure was used to compute TSDI from GRACE and MERRA TWS changes in order to explore hydrological droughts over the GHA for the entire study period (1980-2014).

[FIGURE 2 AROUND HERE.]

[TABLE 2 AROUND HERE.]

4.3. Spatial Independent Component Analysis (sICA)

The sICA (Forootan & Kusche, 2012) approach was applied to extract statistically independent modes of precipitation and TWS changes. We emphasize that sICA patterns are essentially regions with similar seasonality (and not typical spatial patterns of variability) and as such, there could be significant bias in the analysis from the wettest stations. As the estimated modes are statistically independent, they can be separately analysed without considering other modes (see an application of sICA over the Nile Basin in Awange et al., 2014a). Suppose $\mathbf{X}(t, s)$ is a gridded time series of precipitation or TWS changes after removing their dominant annual and semi-annual cycles. sICA decomposes the time-series of $\mathbf{X}$ into j spatial $\mathbf{S}_j$ and temporal $\mathbf{A}_j$ modes as:

$$\mathbf{X}(t, s) = \mathbf{A}_j(t)\ \mathbf{S}_j(s), \tag{4}$$

where t is the time and s represents the grid points. By applying sICA the rows of $\mathbf{S}$ are statistically as independent as possible, and the columns of $\mathbf{A}$ are their corresponding temporal evolutions. The use of sICA as opposed to principal component analysis (PCA) or its rotated version (RPCA) makes sense in this study since it helps to identify (or localize) specific hydrological areas impacted by droughts or extreme wet conditions over GHA, which is not possible when using PCA or RPCA. The details of sICA estimation are reported in Forootan (2014), chapter 4. Here, only the first four dominant modes of both precipitation and TWS changes were found statistically significant and consequently were considered separately to reconstruct precipitation and TWS changes over various sub-regions of GHA. Both SPI and TSDI (as discussed in Sections 4.1 and 4.2) were estimated using the four dominant sICA modes.

5. Results and Discussions

5.1. Changes in Precipitation and TWS

Changes in TWS depend on the variability of precipitation and climate extremes. Rainfall over GHA region has been reported to show considerable inter-seasonal and inter-annual variability over the past few decades beside the long-term changes (e.g., Williams et al., 2012; Lyon, 2014; Omondi et al., 2014). Figure 3 shows the variability of rainfall and TWS changes. Trends were estimated from monthly rainfall/TWS anomalies (y) over various common time periods (T) using multilinear regression technique ($y =$

$\hat{\beta}_0 + \hat{\beta}_1 T + \hat{\beta}_2.\sin(2\pi T) + \hat{\beta}_3.\cos(2\pi T) + \hat{\beta}_4.\sin(4\pi T) + \hat{\beta}_5.\cos(4\pi T) + \epsilon(T))$, where $\hat{\beta}_0$ is a constant term, $\hat{\beta}_1$ represents the linear trend, and the remaining terms represent the annual and semi-annual signals, ϵ represents the error terms. Only changes that are significant at 95% confidence interval based on student's t-test are shown.

Figure 3(a) shows significant decline (up to 20 mm/decade) in rainfall over southern and northern Sudan as well as increase in rainfall over central Ethiopia between 2002 and 2014 based on monthly TRMM precipitation estimates. Equivalent increase (decrease) in TWS over central Ethiopia (eastern Kenya, Somalia, and northern Sudan) are noted in MERRA (Figure 3b). GRACE also indicated decreasing trends over southern Sudan and eastern Kenya (similar to rainfall) as well as anomalously large positive trends (up to 20 mm/year) over the Lake Victoria region (Figure 3c). However, a completely opposite sign is observed in the long-term records of GPCC precipitation products between 1980 and 2010 (Figure 3d; i.e., multidecadal oscillations may be influencing the sign of the trends), which indicate significant negative (positive) changes over Ethiopia and Tanzania (Sudan and Somalia). This might have lead to a overall negative trend in TWS over the northern parts of GHA during the same period as shown by MERRA in Figure 3e.

[FIGURE 3 AROUND HERE.]

Figure 4 shows the area-averaged seasonal anomalies of TWS based on MERRA (1980-2014) and GRACE (2002-2014) data. Substantial inter-seasonal variations in TWS over the past 30-40 years are observed. Besides decadal

trends, prolonged periods of negative TWS anomalies in the late 1980s to early 1990s and late 1990s and early 2000s are observed. Although, GRACE data covers a very short time period, the inter-seasonal variations are visible in all the seasons. While the TWS changes in 2009 may have occurred as a result of the historical 2009-2011 drought, TWS changes between 2002 and 2006 at a rate of 6.20 mm/month seen in GRACE data has been linked to other processes such as anthropogenic, evaporations, and rainfall deficiency (Awange et al., 2008, 2014a).

To assess the overall relationship between rainfall and GRACE TWS changes over the region, the temporal correlations are computed and presented in Figure 5, together with their lags. High correlations between rainfall and TWS (with a 2-month time lag) observed in Figure 5a indicate that TWS changes are primarily driven by precipitation. Areas of low correlation (over central GHA region) show a time-lag of about one month (see, Figure 5d). This low correlations could be related to seasonality, where the rainfall is usually bimodal over these regions.

MERRA TWS changes on its part show considerably better correlations with rainfall indicating that TWS changes simulated by MERRA are mainly driven by precipitation (Figure 5b). It should be noted that MERRA does not simulate changes in surface water and groundwater, and therefore, does not represent the integrated changes in TWS as observed by GRACE satellites (Rienecker et al., 2011). The large-scale high correlation patterns observed in Figure 5b are further illustrated by the time lags, where the majority of the region indicated a lag of only one month. Further, the correlations between GRACE and MERRA (Figure 5c) closely resemble those of rainfall

and GRACE, although over a different time lag (see, Figure 5f).

[FIGURE 4 AROUND HERE.]

[FIGURE 5 AROUND HERE.]

5.2. Spatio-temporal Drought Patterns over GHA

To study the temporal drought patterns over the GHA, sICA was applied on the non-seasonal rainfall/TWS anomalies to derive region-specific patterns of temporal variability over the period 1979 to 2014. Figure 6 shows the standard deviations derived from the first four leading modes of rainfall variability, together with their corresponding temporal patterns (ICs). The first independent mode of rainfall variability based on GPCC indicates the largest anomalies over central GHA (Kenya, parts of Ethiopia and Somalia), accounting for 23.8% of the variability (Figure 6a). The second mode (20.2%) is localized over central Ethiopia indicating a maximum standard deviation of about 30 mm (Figure 6b) while the third mode (20.0%) is concentrated over Tanzania (Figure 6c). The fourth mode (13.3%) is localized over northern Ethiopia and Sudan (Figure 6d). TRMM showed similar spatial patterns to GPCC (Figure 6e-h) except that the second and third modes were inter-changed (cf. that of GPCC in Figures 6b and 6c). The maximum variability in the third mode was found to be localized completely over Ethiopia (Figures 6g-h).

The corresponding temporal patterns in Figures 6i-l, indicate considerable inter-annual variability and their temporal variations appeared to be considerably different from each other signifying the complexity of the re-

gion. Note that the ICs are only shown for the period 1998 to 2014 in order to highlight the differences between the two precipitation products.

The four dominant modes of TWS variability are shown in Figure 7 with both MERRA (1980-2014) and GRACE (2002-2014) indicating distinct patterns of maximum variability over various parts of the GHA region. In order to highlight the differences in temporal evolutions between MERRA and GRACE, the ICs are plotted from 2002 to 2014 only. MERRA TWS showed the largest anomalies over western Ethiopia (explaining about 30% of the variability; Figure 7a) while the second mode (18.2%) is localized over western Tanzania (Figure 7b). The third independent mode showed maximum variations over the northern Lake Victoria region accounting for 17.3% of the variability (Figure 7c). The fourth mode (14.3%) is mainly concentrated over South Sudan (Figure 7d).

GRACE showed maximum variability ($\sim$27%) over the Lake Victoria region (Figure 7e). Its second mode (16%) indicates maximum variations between Sudan and Ethiopia (Figure 7f) while its third mode ($\sim$14%) is localized over South Sudan (Figure 7g). The fourth mode (13.8%), although not very distinctive in its spatial pattern, shows a similar temporal pattern to that of MERRA over Tanzania. It should be noted here that the spatial patterns of maximum variability shown by MERRA do not exactly match with those from GRACE data. This could be possibly due to limitations in MERRA (errors in TWS modelling) and GRACE data (short time period). One obvious limitation in MERRA lies in its inability to capture the maximum variations resulting from the Lake Victoria Basin (see, e.g., sICA 1 in Figure 7e). Note though that for GHA, the regions of maximum variations

often overlap among the four leading modes. For example, the maximum variations over South Sudan shown by MERRA (Figure 7d) matche quite well with sICA 3 of GRACE data (see, Figure 7g).

In this way, we match the spatial patterns of sICA from GRACE and MERRA to plot their ICs in Figures 7i-l. It can be seen that the matched temporal patterns between GRACE and MERRA are very close. The corresponding ICs plotted between 2002 and 2014 show considerably inter-annual variability, indicating the hydrological extremes over parts of the GHA region. For example, the temporal patterns over the Lake Victoria region (Figure 7e) are reproduced reasonably well by GRACE and MERRA (Figure 7i), indicating a rapid decline in TWS from 2002 to 2006 and steadily increasing thereafter (see e.g., Awange et al., 2008; Swenson & Wahr, 2009). GRACE (IC2, Figure 7j, Ethiopia-Sudanese border) indicates the typical hydrological extremes, i.e., droughts of 2004, 2009, and 2011 while GRACE (IC3) fairly representes the dry periods over South Sudan (Figure 7k). GRACE (IC4), which is mainly localized over the eastern GHA region (Figure 7l) indicates a rapid decline of TWS from 2002 to 2006 and 2007 to 2010.

[FIGURE 6 AROUND HERE.]

[FIGURE 7 AROUND HERE.]

Based on the sICA results in Figures 6 and 7, in Table 3, we classified GHA into four sub-regions in the order of sICA-derived patterns of GRACE TWS in Figures 7e-h. Precipitation and TWS anomalies reconstructed from the individual spatial and temporal modes provide rainfall and TWS changes with anomalies mainly localized over these four regions. Four time-series were

calculated for each dataset based on the four leading sICA modes to generate SPI and TSDI indices used to study the hydrological extremes over the period 1980 to 2014. Since we have already removed the seasonal component from both precipitation and TWS changes before applying the sICA, it is not necessary to use Eq. 1 to compute the TSD anomalies. Instead, we converted the TWS anomalies to TSD (in %) by dividing them with the range (TWS_{max}-TWS_{min}). While SPI is straight forward (Figure 8), the calculation of TSDI index is rather complicated depending on the period of drought events, which is important for deriving the slope and y-intercept parameters from the cumulative TSDs. By analyzing the individual time-series, we estimated the TSDIs for all the four regions and plotted them in Figure 9. For example, TSDI (of GRACE TWS) over Lake Victoria region (Region 1) was calculated from cumulative TSDs between June 2006 and November 2006 while the TSDI over South Sudan (Region 3) was calculated for August 2009 to May 2010 (see Table 3).

[TABLE 3 AROUND HERE.]

Figure 8 shows the 12-month SPI indices calculated from GPCC (1979-2010) and TRMM (1998-2014) over the four regions as indicated in Table 3 and Figures 7e-h. These are (a) Region 1 covering the Lake Victoria Basin, (b) Region 2, including the Ethiopia-Sudan border, (c) Region 3 covering South Sudan, and (d) Region 4, including Tanzania and parts of Ethiopia. The first 12 months of GPCC (i.e., 1979) and TRMM (i.e., 1998) were removed during the SPI computation. Table 4 summarizes the duration and intensity of severe to extreme meteorological drought episodes for the four

sub-regions between 1980 and 2014. The SPI indices over Region 1 in Figure 8a (corresponding to Figures 6a and 6e) shows extreme drought events in 1984, 1999-2000, 2009, and 2011, consistent with the findings in Lyon (2014). The most notable droughts over Ethiopia and eastern Sudan (Region 2, Table 3) include the extreme drought events of 2009 and some moderate droughts in 1984, 1986, 1992, 1994,and 2002 (Figure 8b). SPI patterns over South Sudan (Figure 8c, see also, Table 3) indicate prolonged droughts from 1982 to early 1985 and between 2009 and 2010. The SPI indices over Tanzania (Region 4, Figure 8d) indicate considerable variability with severe/extreme droughts lasting from one to two years (e.g., 1988-1989, 1997-1998, 2003-2004, and 2005-2006).

Although there were indications of decreasing rainfall from 1980-1982, it did not lead to extreme droughts over Tanzania. The region exhibited only a moderate drought from 2010-2011, which caused devastating affects in other parts of the GHA (WMO, 2012; Tierney et al., 2013). The two precipitation products, GPCC and TRMM were found to be fairly consistent across all the four regions between 1998 and 2010 but were found to differ slightly over Region 3 (over South Sudan, Figure 8c), where rainfall variability of GPCC was highest over central Sudan and northern Ethiopia (see, Figure 6d) in contrast to South Sudan as indicated by TRMM (Figure 6g).

[FIGURE 8 AROUND HERE.]

[TABLE 4 AROUND HERE.]

Figure 9 shows the TSDIs of the four regions (see Table 3). Major hydrological drought events between 1980 and 2014 based on TWS changes de-

rived from MERRA (1980-2014) and GRACE (2002-2014) are summarized in Table 5. For MERRA, only severe to extreme droughts are shown for brevity. Clearly, three or more severe to extreme hydrological droughts occurred over various regions of GHA with some of them lasting for 75 months (Table 5). Over the Lake Victoria Basin, especially over Kenya and northern Tanzania, four major droughts were detected, which in total lasted for 20 or more months (Figure 9a). All the four droughts occurred as a result of prolonged meteorological dry episodes (see, Table 4) over the same region. While MERRA indicated only moderate droughts from 2004-2006, GRACE showed severe droughts from March 2004 to November 2006, which lasted for 33 months, the period that coincided with the fall of Lake Victoria water level between 2002 and 2006 due to the expansion of the Owen Falls Dam (see e.g., Awange et al., 2008). From Table 4 (see also, Figure 8d), it can be seen that a severe meteorological drought also occurred from October further exacerbating the TWS decline. However, the most recent extreme meteorological droughts of 2009-2010 and 2010-2011 (see, Table 4) only caused moderate hydrological droughts over the region (Table 5).

[FIGURE 9 AROUND HERE.]

[TABLE 5 AROUND HERE.]

Over Ethiopia and Sudan (Region 2), we observe very different scenarios of TWS variability between GRACE and MERRA especially over 2002 to 2014, where GRACE data showed large positive (negative) TSDIs between 2007 and 2009 (2007 and 2011), which were not represented well by MERRA (Figure 9b). MERRA also indicates prolonged droughts from April 2000 to

June 2006 lasting for about 75 months (Figure 9b and Table 5), which we believe could be spurious. However, it is also observed that two meteorological droughts have occurred (1999-2000, and 2002-2004), which might have affected the TWS variability in MERRA. Extreme hydrological droughts have been found from July 2011-July 2012 (MERRA) and September 2009-October 2011 (GRACE) in response to the prolonged meteorological drought conditions over the region (see, Figure 9b). MERRA also indicated extreme droughts between 1990 and 1993, which was again, in response to the meteorological droughts that occurred from 1991-1992. The region also experienced the largest TWS decline (extreme hydrological drought) in 2009-2010 and 2010-2011, corresponding to the historical drought events from 2009-2011. These events were well-captured by the two precipitation products (Figure 8b) and GRACE-derived TWS changes (Figure 9b). During this two periods, SPI dropped below -2.5 while the TSDI was round -6.0 during the peak period (i.e., December to February 2009-2010). It is also interesting to observe that both the meteorological droughts eventuated from rainfall deficits during the OND season.

TSDI patterns over Region 3 representing the South Sudan region are quite complicated as both GRACE and MERRA indicate high intra-seasonal variability (especially observed in GRACE) but the extreme drought of 2011-2012 was well captured by GRACE (Figure 9c). This could have occurred as a result of prolonged meteorological droughts that last for 39 months from May 2009 to July 2012. Note that MERRA also indicated prolonged hydrological droughts between July 1988 and December 1992. Region 4 covering Tanzania and parts of Ethiopia experienced several instances of droughts with

varying intensities between 1980 and 2014 (Figure 9d). The most notable drought events shown by MERRA are the prolonged droughts that occurred in the early 1990, the late 1990s, and in 2011. Similar to the Lake Victoria Basin (Region 1), this region also exhibited significant decline in TWS from 2003 to mid-2006 leading to a prolonged (and extreme) hydrological drought over the region. It should be noted here that the region also suffered two meteorological droughts (2003-2004 and 2005-2006) during the period (see, Figure 8d). The 2010-2011 extreme drought was also captured very well by GRACE data.

Figure 10 illustrates the spatial evolution of the 2009-2010 drought computed as a sum of rainfall/TWS over three important seasons. It is observed that the entire GHA experienced anomalously low rainfall during OND 2010 (Figure 10a), which remained relatively dry during MAM 2011 over Kenya, Ethiopia, and South Sudan (Figure 10b) before recovering to positive changes. TWS anomalies were mostly negative in the southern and western parts of GHA during OND 2010 (Figure 10d) but their magnitudes further increased during MAM 2011 (Figure 10e). High negative anomalies have shifted to Region 3 during JJAS 2011 but the majority of the regions still indicate negative anomalies (Figure 10f) as a result of deficit rainfall in the two preceding months.

[FIGURE 10 AROUND HERE.]

It is observed that almost all the hydrological droughts over the GHA region have resulted from extreme (and/or prolonged) meteorological droughts with both SPI and TSDI indicating consistent temporal variability during

the period 1980-2014. To illustrate the relationship between SPI and TSDI, we plot the SPI and TSDI values based on TRMM precipitation estimates (1998-2014) and GRACE-derived TWS changes (2002-2014) for the period 1999 to 2014 in Figure 11, with TSDI values scaled to the SPI values. The temporal patterns of SPI and TSDI are closely matched for Region 1, 3, and 4 while the major drought events of 2009-2010 and 2010-2011 over Region 2 were also represented well by SPI and TSDI, where hydrological droughts have occurred almost 5-6 months after the meteorological drought.

The correlations between SPI and TSDI were computed for the period 2002-2014 (Table 6). Consistent with Figure 11, we found significant correlations (at 95% confidence interval) between SPI and TSDI during the period with a correlation of 0.44 (at one month lag), 0.52 (at 3 month lag), and 0.59 (at one month lag) for Region 1, Region 3, and Region 4, respectively. The correlation between SPI and TSDI for Region 2 was not significant. There exists a high seasonal correlation over the region between rainfall and TWS changes (see, Figure 5a). The correlations between MERRA-derived TSDI and GRACE-derived TSDI were found to be significant over all the four regions with a lag of up to 1 month (see, Table 6). In quantifying changes in TWS and the resulting hydrological drought events (as indicated by TSDI) in GHA, contributions due to evapotranspiration and increased use of freshwater (groundwater and surface water) in the region should be taken into account.

[FIGURE 11 AROUND HERE.]

[TABLE 6 AROUND HERE.]

The study further explored global teleconnection relationships to SPI and TSDI indices. Table 7 shows the correlation coefficients and time lags (in months) between SPI (and TSDI) indices and Niño3.4 and the Dipole Mode Index (DMI) over various time periods between 1979 to 2014. Both SPI and TSDI (GRACE) of Region 1 are significantly correlated with ENSO and IOD and are more related to IOD than ENSO (with a maximum correlation of 0.53 between TRMM and DMI). SPI (GPCC) and TSDI (GRACE) also show significant correlations with ENSO (IOD) while both SPI and TSDI over Region 4 show significant correlations with IOD with the highest correlation of 0.41 for the GRACE-derived TSDI. SPI and TSDI over Region 3 (representing South Sudan) show the least correlation against ENSO (IOD) indicating that rainfall and TWS variability over South Sudan was not associated with large-scale climate events as the region is located further inland compared to the other three regions.

It is observed that MERRA product shows low but opposite correlations with ENSO (IOD) compared to GRACE, which could be another limitation of the reanalysis product. Furthermore, IOD is seen to be the leading driver of rainfall and TWS variability especially over the eastern GHA region with the highest impact over Tanzania and Lake Victoria (see, Table 7). This is consistent with previous studies, which reported that the East African climate is highly governed by the Indian Ocean SST variability (e.g., Williams & Funk, 2011; Tierney et al., 2013; Lyon, 2014).

[TABLE 7 AROUND HERE.]

6. Summary and Conclusions

The study found significant changes in long-term and decadal rainfall based on monthly estimates from GPCC and TRMM over 1979 to 2014. Long-term rainfall changes between 1980 and 2010 indicated significant positive (negative) changes over Sudan (Ethiopia and Tanzania) while changes from 2002 to 2014 showed completely opposite trends over these two regions.

GRACE-derived TWS changes showed high positive (negative) trends over central GHA (South Sudan and Tanzania) with a maximum increase of about 20 mm/yr over the Lake Victoria Basin and central Ethiopia. High correlations (up to 0.9) were noted between monthly rainfall and GRACE TWS changes over South Sudan, western Ethiopia, and Tanzania, with a lag of 1-2 months while rainfall over arid and semi-arid regions such as northern Sudan and Somalia were least correlated, indicating that large-scale variations of TWS are mainly influenced by seasonal rainfall variations.

SPI and TSDI indices estimated over the four sICA-derived spatial regions (Lake Victoria Basin, Ethiopia-Sudanese border, South Sudan, and Tanzania) indicated several instances of severe to extreme meteorological droughts (SPI <1.5) resulting in extreme hydrological droughts that were observed in MERRA and GRACE TWS changes (indicated by TSDIs). Correlations between meteorological droughts (SPI) and hydrological droughts (GRACE-derived TSDI) were found to be significant especially over Lake Victoria region (0.44), Tanzania (0.52), and South Sudan (0.59), signifying that precipitation plays an important role in the hydrological budget of the regions.

While the Lake Victoria Basin experienced six major meteorological droughts

between 1979 and 2014, South Sudan and Ethiopia suffered seven meteorological droughts lasting between one year to 3 and half years. The impact of prolonged meteorological droughts is clearly evident in the TWS changes over all the four regions, which resulted in multiple years of hydrological droughts.

Consistent with the previous studies (e.g., Tierney et al., 2013), the Indian Ocean SST variations were found to play a larger influence on the regional TWS changes ompared to the ENSO mode. It should be noted here that correlations between MERRA and ENSO (IOD) indices were considerably lower (and often opposite). Further verifications are required to assess the quality of reanalysis products to study the long-term changes and hydrological extremes over the GHA region.

Acknowledgments

The authors are grateful for the comments provided by Prof. Paolo D'Odorico (Editor) and the three anonymous reviewers, which considerably improved the quality of this study. J. Awange is grateful to Alexander von Humboldt Foundation, Japan Society of Promotion of Science, Brazilian Science Without Borders Program/CAPES Grant No. 88881.068057/2014-01 which supported his stay in Germany, Japan and Brazil respectively. Khandu is grateful to Curtin Strategic International Research Scholarship, the Intergovernmental Panel on Climate Change (IPCC), and Brazilian Science Without Borders Program/CAPES Grant No. 88881.068057/2014-01 for their valuable scholarships. M. Schumacher appreciates the financial supports by the German Research Foundation (DFG) under the project BAYES-G and

595 also the exchange grant (2015/16 57044996) awarded by the German Aca-
596 demic Exchange Service (DAAD) to visit the Australian National University
597 (ANU). E. Forootan would like to thank the WASM/TIGeR research fellow-
598 ship grant provided by Curtin University (Australia). Special thanks to Dr.
599 Freddie Mpelasoka who provided valuable suggestions and comments on the
600 manuscript. The authors however take full responsibility of the content. Last
601 but not least, we acknowledge GeoForschungsZentrum (GFZ), the National
602 Aeronautics and Space Administration (NASA), and the Global Precipita-
603 tion Climatology Center (GPCC) for providing the necessary datasets used
604 in this study.

References

Agboma, C., Yirdaw, S., & Snelgrove, K. (2009). Intercomparison of the total storage deficit index (tsdi) over two canadian prairie catchments. *Journal of Hydrology*, *374*, 351–359. doi:10.1016/j.jhydrol.2009.06.034.

Andersen, O. B., Seneviratne, S. I., Hinderer, J., & Viterbo, P. (2005). GRACE derived terrestrial water storage depletion associated with the 2003 european heat wave. *Geophysical Research Letters*, *32*, n/a–n/a. doi:10.1029/2005GL023574.

Awange, J., Ferreira, V., Khandu, Andam-Akorful, S., Forootan, E., Agutu, N., & He, X. (2015). Uncertainties in remotely-sensed precipitation data over Africa. *International Journal of Climatology*, . doi:10.1002/joc.4346.

Awange, J., Forootan, E., Kuhn, M., Kusche, J., & Heck, B. (2014a). Water storage changes and climate variability within the Nile basin between 2002 and 2011. *Advances in Water Resources*, *73*, 1–15. doi:10.1016/j.advwatres.2014.06.010.

Awange, J., Gebremichael, M., Forootan, E., Wakbulcho, G., Anyah, R., Ferreira, V., & Alemayehu, T. (2014b). Characterization of Ethiopian mega hydrogeological regimes using GRACE, TRMM and GLDAS datasets. *Advances in Water Resources*, *74*, 64–78. doi:10.1016/j.advwatres.2014.07.012.

Awange, J. L., Anyah, R., Agola, N., Forootan, E., & Omondi, P. (2013). Potential impacts of climate and environmental change on the stored water of

628 lake victoria basin and economic implications. *Water Resources Research*,
629 *49*, 8160–8173. doi:10.1002/2013WR014350.

630 Awange, J. L., Mohammad, S., Ogonda, G., Wickert, J., Grafarend, E., , &
631 Omullo, M. (2008). The falling lake victoria water level: Grace, trimm and
632 champ satellite analysis of the lake basin. *Water Resource Management*,
633 *22*, 775–796. doi:10.1007/s11269-007-9191-y.

634 Chen, J. L., Wilson, C. R., Tapley, B. D., Longuevergne, L., Yang, Z. L., &
635 Scanlon, B. R. (2010). Recent la plata basin drought conditions observed
636 by satellite gravimetry. *Journal of Geophysical Research: Atmospheres*,
637 *115*, n/a–n/a. doi:10.1029/2010JD014689.

638 Chen, J. L., Wilson, C. R., Tapley, B. D., Yang, Z. L., & Niu, G. Y. (2009).
639 2005 drought event in the Amazon River basin as measured by GRACE
640 and estimated by climate models. *Journal of Geophysical Research: Solid*
641 *Earth*, *114*, n/a–n/a. doi:10.1029/2008JB006056.

642 Cheng, M. K., Ries, J. C., & Tapley, B. D. (2013). Geocenter variations from
643 analysis of slr data. In *Reference Frames for Applications in Geosciences*
644 (pp. 19–25). Springer Berlin Heidelberg volume 138 of *International As-*
645 *sociation of Geodesy Symposia*.

646 Cheng, M. K., & Tapley, B. D. (2004). Variations in the earth's oblateness
647 during the past 28 years. *Geophysical Research Letters*, *109*. doi:10.1029/
648 2004JB003028.

649 Dahle, C., Flechtner, F., Gruber, C., König, D., König, R., Michalak, G., &
650 Neumayer, K.-H. (2013). *GFZ GRACE Level–2 Processing Standards Doc-*

ument for Level–2 Product Release 0005: revised edition, January 2013. Scientific Technical Report STR12/02 – Data, rev. ed. Deutsches GeoForschungsZentrum GFZ Potsdam. doi:10.2312/GFZ.b103-1202-25.

Forootan, E. (2014). *Statistical Signal Decomposition Techniques for Analyzing Time-Variable Satellite Gravimetry Data*. Ph.D. thesis University of Bonn, Germany. doi:http://hss.ulb.uni-bonn.de/2014/3766/3766.htm.

Forootan, E., Awange, J., Kusche, J., Heck, B., & Eicker, A. (2012). Independent patterns of water mass anomalies over Australia from satellite data and models. *Remote Sensing of Environment*, *124*, 427–443. doi:10.1016/j.rse.2012.05.023.

Forootan, E., & Kusche, J. (2012). Separation of global time-variable gravity signals into maximally independent components. *Journal of Geodesy*, *86*, 477–497. doi:10.1007/s00190-011-0532-5.

Forootan, E., & Kusche, J. (2013). Separation of deterministic signals using independent component analysis (ICA). *Studia Geophysica et Geodaetica*, *57*, 17–26. doi:10.1007/s11200-012-0718-1.

Funk, C., Hoell, A., Shukla, S., Bladé, I., Liebmann, B., Roberts, J. B., Robertson, F. R., & Husak, G. (2014). Predicting East African spring droughts using Pacific and Indian ocean sea surface temperature indices. *Hydrol. Earth Syst. Sci. Discuss.*, *11*, 3111–3136. doi:10.5194/hessd-11-3111-2014.

673 Houborg, R., Rodell, M., Li, B., Reichle, R., & Zaitchik, B. F. (2012).
674 Drought indicators based on model-assimilated Gravity Recovery and Cli-
675 mate Experiment (GRACE) terrestrial water storage observations. *Water*
676 *Resources Research*, *48*. doi:10.1029/2011WR011291.

677 Huffman, G. J., Bolvin, D. T., Nelkin, E. J., Wolff, D. B., Adler, R. F.,
678 Gu, G., Hong, Y., Bowman, K. P., & Stocker, E. F. (2007). The
679 TRMM multisatellite precipitation analysis (TMPA): Quasi-global, mul-
680 tiyear, combined-sensor precipitation estimates at fine scales. *Journal of*
681 *Hydrometeorology*, *8*, 38–55. doi:10.1175/JHM560.1.

682 Kurnik, B., Barbosa, P., & Vogt, J. (2011). Testing two different precipitation
683 datasets to compute the standardized precipitation index over the Horn of
684 Africa. *International Journal of Remote Sensing*, *32*, 5947–5964. doi:10.
685 1080/01431161.2010.499380.

686 Kusche, J., Schmidt, R., Petrovic, S., & Rietbroek, R. (2009). Decorrelated
687 grace time-variable gravity solutions by gfz, and their validation using a
688 hydrological model. *Journal of Geodesy*, *83(10)*, 903–913. doi:10.1007/
689 s00190-009-0308-3.

690 Landerer, F. W., & Swenson, S. C. (2012). Accuracy of scaled GRACE
691 terrestrial water storage estimates. *Water Resources Research*, *48*. doi:10.
692 1029/2011WR011453.

693 Leblanc, M. J., Tregoning, P., Ramillien, G., Tweed, S. O., & Fakes, A.
694 (2009). Basin-scale, integrated observations of the early 21st century mul-

tiyear drought in southeast australia. *Water Resources Research*, *45*, n/a–n/a. doi:10.1029/2008WR007333.

Li, B., & Rodell, M. (2014). Evaluation of a model-based groundwater drought indicator in the conterminous U.S. *Journal of Hydrology*, *526*, 78–88. doi:10.1016/j.jhydrol.2014.09.027.

Long, D., Scanlon, B. R., Longuevergne, L., Sun, A. Y., Fernando, D. N., & Save, H. (2013). GRACE satellite monitoring of large depletion in water storage in response to the 2011 drought in Texas. *Geophysical Research Letters*, *40*, 33953401. doi:10.1002/grl.50655.

Lyon, B. (2014). Seasonal drought in the Greater Horn of Africa and its recent increase during the March-May long rains. *Journal of Climate*, *27*, 79537975. doi:10.1175/JCLI-D-13-00459.1.

Marthews, T. R., Otto, F. E. L., Mitchell, D., Dadson, S. J., & Jones, R. G. (2015). The 2014 drought in the horn of africa: Attribution of meteorological drivers. *Bull. Amer. Meteor. Soc.*, *96*, 8388. doi:http://dx.doi.org/10.1175/BAMS-EEE_2014_ch17.1.

McKee, T., Doesken, N. J., & Kliest, J. (1993). The relationship of drought frequency and duration to time scales. In *Proceedings of the 8th Conference of Applied Climatology, 17-22 January, Anaheim, CA* (pp. 194–184). American Meterological Society, Boston, MA.

McKee, T., Doesken, N. J., & Kliest, J. (1995). Drought monitoring with multiple time scales. In *9th AMS Conference on Applied Climatology* (pp. 233–236). American Meterological Society, Boston, MA.

718 Narasimhan, B., & Srinivasan, R. (2005). Development and evaluation of
719 Soil Moisture Deficit Index (SMDI) and Evapotranspiration Deficit Index
720 (ETDI) for agricultural drought monitoring. *Agricultural and Forest Me-*
721 *teorology*, *133(1-4)*, 6988. doi:10.1016/j.agrformet.2005.07.012.

722 Naumann, G., Dutra, E., Barbosa, P., Pappenberger, F., Wetterhall, F.,
723 , & Vogt, J. V. (2014). Comparison of drought indicators derived from
724 multiple data sets over Africa. *Hydrology and Earth System Sciences*, *18*,
725 1625–1640. doi:10.5194/hess-18-1625-2014.

726 Nicholson, S. E. (1997). An analysis of the enso signal in the tropical at-
727 lantic and western INDIAN oceans. *International Journal of Climatol-*
728 *ogy*, *17*, 345375. doi:10.1002/(SICI)1097-0088(19970330)17:4<345::
729 AID-JOC127>3.0.CO;2-3.

730 Omondi, P. A., Awange, J. L., Forootan, E., Ogallo, L. A., Barakiza, R.,
731 Girmaw, G. B., Fesseha, I., Kululetera, V., Kilembe, C., Mbati, M. M.,
732 Kilavi, M., King'uyu, S. M., Omeny, P. A., Njogu, A., Badr, E. M., Musa,
733 T. A., Muchiri, P., Bamanya, D., & Komutunga, E. (2014). Changes in
734 temperature and precipitation extremes over the greater horn of africa
735 region from 1961 to 2010. *International Journal of Climatology*, *34*, 1262–
736 1277. doi:10.1002/joc.3763.

737 Palmer, W. (1965). *Meteorological drought*. Technical Report Research
738 Paper 45 US Department of Commerce, Weather Bureau Washington
739 DC. Available at: https://www.ncdc.noaa.gov/temp-and-precip/
740 drought/docs/palmer.pdf.

741 Rienecker, M. M., Suarez, M. J., Gelaro, R., Todling, R., Bacmeister, J., Liu,
742 E., Bosilovich, M. G., Schubert, S. D., Takacs, L., Kim, G. K., Bloom, S.,
743 Chen, J., Collins, D., Conaty, A., da Silva, A., Gu, W., Joiner, J., Koster,
744 R. D., Lucchesi, R., Molod, A., Owens, T., Pawson, S., Pegion, P., Redder,
745 C. R., Reichle, R., Robertson, F. R., Ruddick, A. G., Sienkiewicz, M., &
746 Woollen, J. (2011). Merra: Nasas modern-era retrospective analysis for
747 research and applications. *Journal of Climae*, *24*, 36243648. doi:10.1175/
748 jcli-d-11-00015.1.

749 Schneider, U., Becker, A., Finger, P., Meyer-Christoffer, A., Ziese, M., &
750 Rudolf, B. (2014). GPCC's new land surface precipitation climatology
751 based on quality-controlled in situ data and its role in quantifying the
752 global water cycle. *Theoretical and Applied Climatology*, *115*, 15–40.
753 doi:10.1007/s00704-013-0860-x.

754 Sheffield, J., Wood, E. F., Chaney, N., Guan, K., Sadri, S., Yuan, X., Olang,
755 L., A., Amani, Ali, A., Demuth, S., & Ogallo, L. (2014). A drought
756 monitoring and forecasting system for Sub-Sahara African water resources
757 and food security. *Bull. Amer. Meteor. Soc.*, *95*, 861–882. doi:10.1175/
758 BAMS-D-12-00124.1.

759 Swenson, S., & Wahr, J. (2009). Monitoring the water balance of lake
760 victoria, east africa, from space. *Journal of Hydrology*, *370*, 163–176.
761 doi:10.1016/j.jhydrol.2009.03.008.

762 Tapley, B. D., Bettadpur, S., Watkins, M., & Reigber, C. (2004). The grav-
763 ity recovery and climate experiment: Mission overview and early results.
764 *Geophysical Research Letters*, *33*. doi:10.1029/2004GL019779.

765 Thomas, A. C., Reager, J. T., Famiglietti, J. S., & Rodell, M. (2014). A
766 GRACE-based water storage deficit approach for hydrological drought
767 characterization. *Geophysical Research Letters*, *41*, 1537–1545. doi:10.
768 1002/2014GL059323.

769 Tierney, J. E., Smerdon, J. E., Anchukaitis, K. J., & Seager, R. (2013).
770 Multidecadal variability in East African hydroclimate controlled by the
771 Indian Ocean. *Nature*, *493*, 389–392. doi:10.1038/nature11785.

772 Viste, E., Korecha, D., & Sorteberg, A. (2013). Recent drought and pre-
773 cipitation tendencies in Ethiopia. *Theoretical and Applied Climatology*,
774 *112(3)*, 535–551. doi:10.1007/s00704-012-0746-3.

775 Wahr, J., Molenaar, M., & Bryan, F. (1998). Time variability of the Earth's
776 gravity field: Hydrological and oceanic effects and their possible detec-
777 tion using GRACE. *Journal of Geophysical Research*, *103*, 30,205–30,229.
778 doi:10.1029/98JB02844.

779 Williams, A. P., & Funk, C. (2011). A westward extension of the warm
780 pool leads to a westward extension of the Walker circulation, dry-
781 ing eastern Africa. *Climate Dynamics*, *37*, 2417–2435. doi:10.1007/
782 s00382-010-0984-y.

783 Williams, A. P., Funk, C., Michaelsen, J., Rauscher, S. A., Robertson, I.,
784 Wils, T. H. G., Eshetu, Z., & Loader, N. J. (2012). Recent summer pre-
785 cipitation trends in the Greater Horn of Africa and the emerging role of
786 Indian Ocean sea surface temperature. *Climate Dynamics*, *39*, 2307–2328.
787 doi:10.1007/s00382-011-1222-y.

WMO (2012). *WMO statement on the status of the global climate in 2011*. Technical Report WMO-No. 1085 World Meteorological Organization Geneva, Switzerland.

Yirdaw, S., Snelgrove, K., & Agboma, C. (2008). GRACE satellite observations of terrestrial moisture changes for drought characterization in the canadian prairie. *Journal of Hydrology*, *356*, 84–92. doi:10.1016/j.jhydrol.2008.04.004.

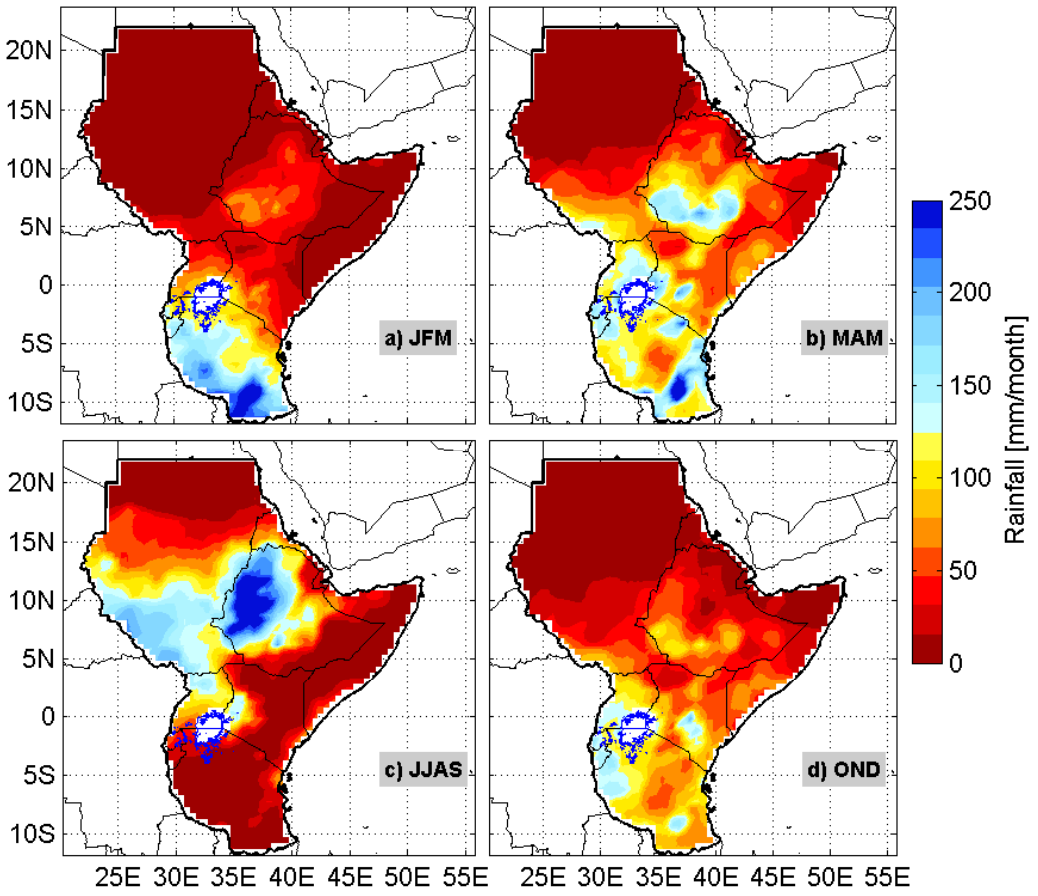

Figure 1: Spatial variability of seasonal rainfall over GHA from 1979-2010 based on GPCC v6 data: a) January-March (JFM), b) March-May (MAM), c) June- September (JJAS), and d) October-December (OND). Note that the signals over Lake Victoria has been masked out in our analysis to avoid spurious trends due to varying lake levels.

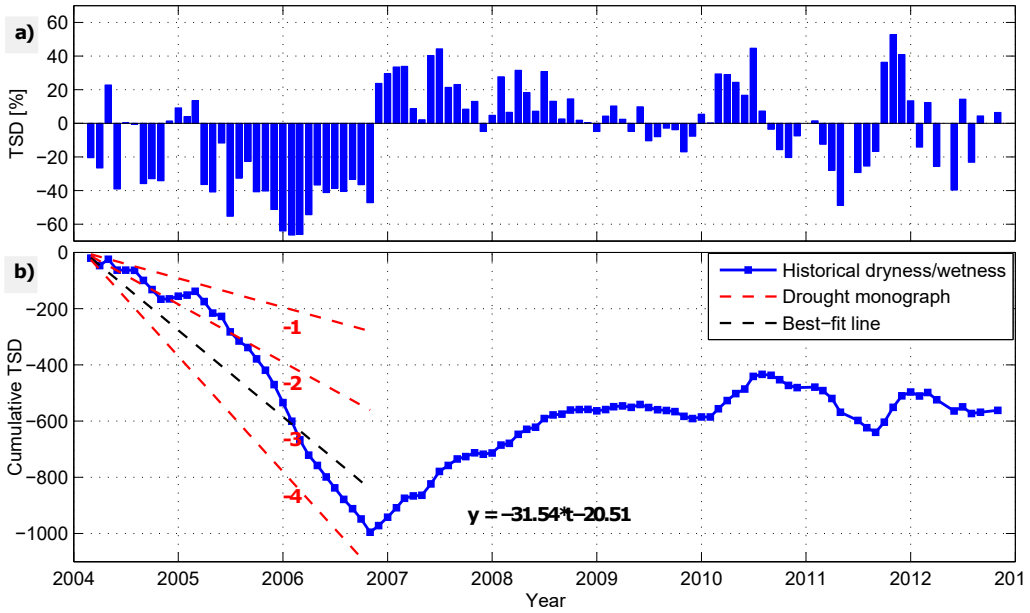

Figure 2: Total storage deficit over eastern GHA region from 2004 to 2013 (a) and cumulative total storage deficit (%) over the same period (b). Considering the horizontal line of zero in the Figure (b) to represent near normal condition, following Palmer (1965) classification, the interval from near normal to severe dryness was divided into four equal intervals, with the part above the best fit line having two lines (1 and 2) and the best fit is shown by line 3. To complete the Palmer (1965) classification, a fourth line 4 was plotted. All the four lines were drawn at equal intervals to define the extreme (Line 4), severe (Line 3), moderate (Line 2), and normal (Line 1) drought conditions.

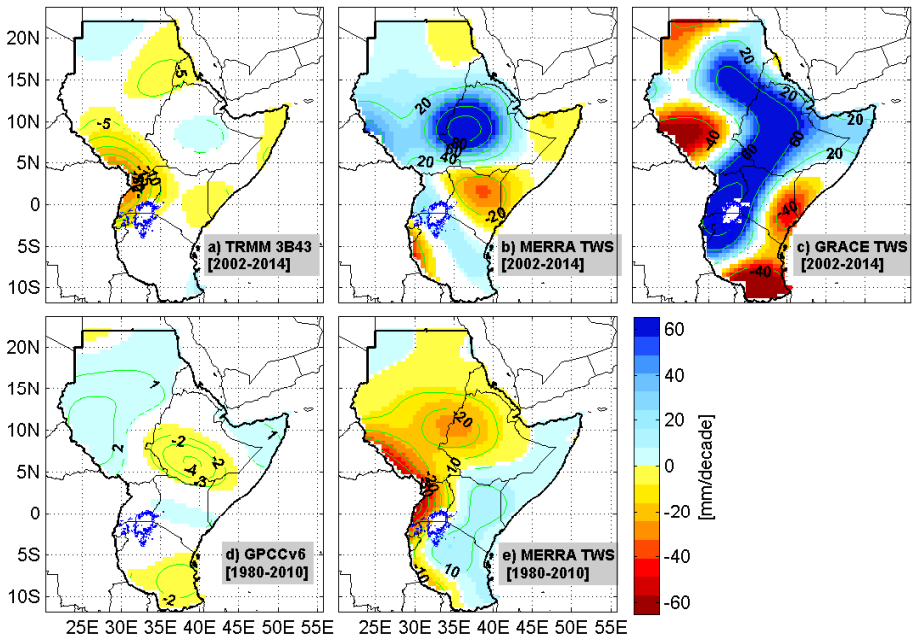

Figure 3: Spatial variability of linear trend over GHA based on a full complement of monthly data at 95% confidence level from 2002-2014 for (a) TRMM rainfall, (b) MERRA TWS, and (c) GRACE TWS. Long term variability are also assessed from 1980-2010 for (d) GPCC rainfall and (e) MERRA TWS. Note that signals over Lake Victoria were not included (i.e., they are masked).

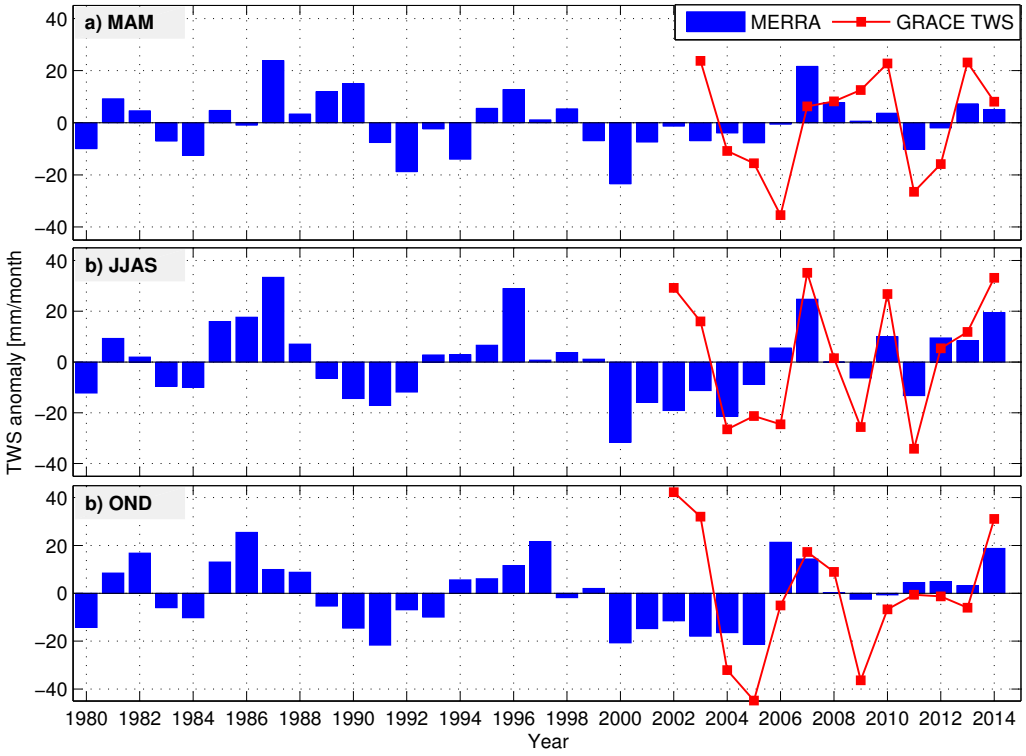

Figure 4: Regional-averaged seasonal anomalies of TWS over the GHA region based on MERRA (1980-2014) and GRACE (2002-2014). The seasonal averages are shown for (a) MAM, (b) JJAS, and (c) OND corresponding to Figures 1b-d.

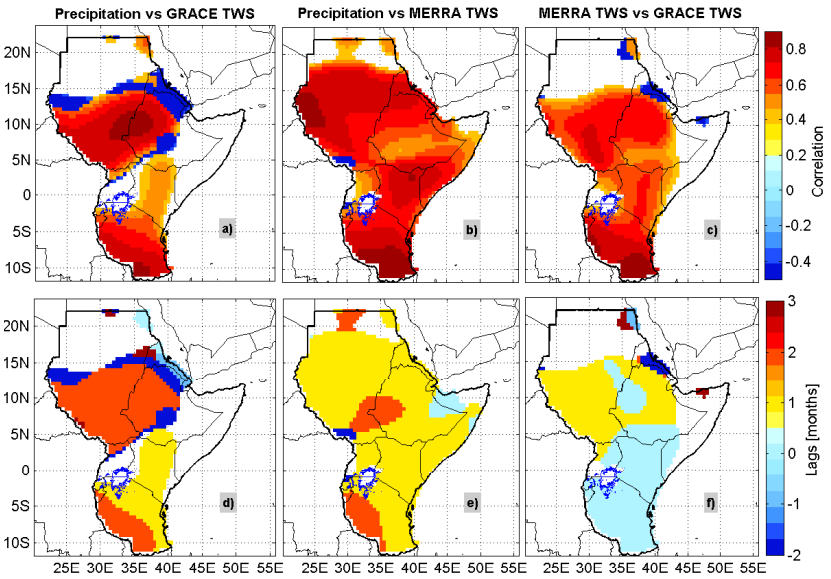

Figure 5: Temporal correlations (with lags in months) between monthly rainfall and TWS changes for the common period 2002-2014. Correlations and lags were computed between a&d) monthly precipitation estimates of TRMM and TWS changes derived from GRACE Level 2 data, b&e) monthly precipitation estimates of TRMM 3B43 and TWS changes simulated MERRA, and c&f) GRACE and MERRA TWS changes over the entire GHA region. Note that the values which are not significant at 95% were not shown.

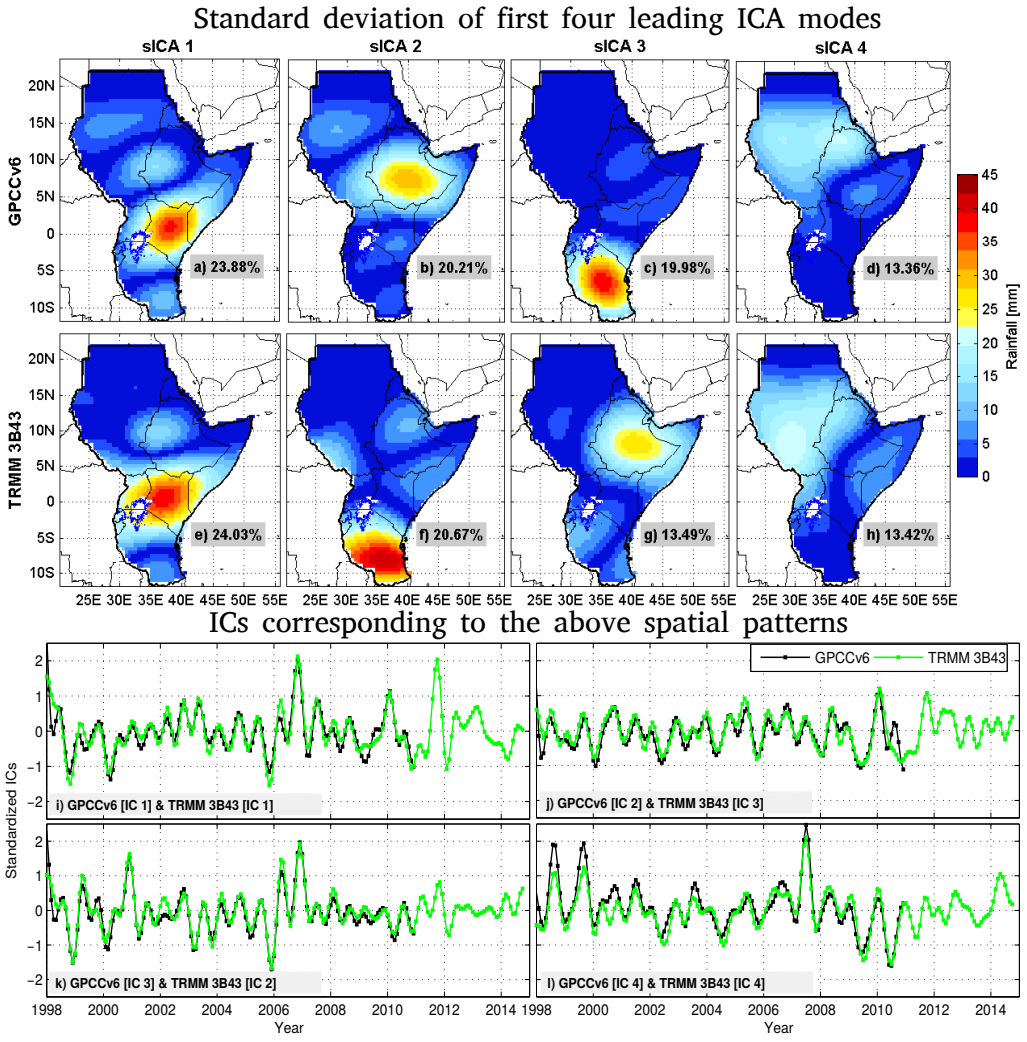

Figure 6: The first four dominant modes of rainfall variability over the GHA region based on a-d) GPCC (1979-2010), and e-h) TRMM (1998-2014). The corresponding temporal patterns (or ICs) are shown in the bottom panels (i-l), where a low-pass filter is applied to enhance their interpretation. (i) Temporal patterns corresponding to a & e, (j) b& g, (k) c & f, and (l) d & h.

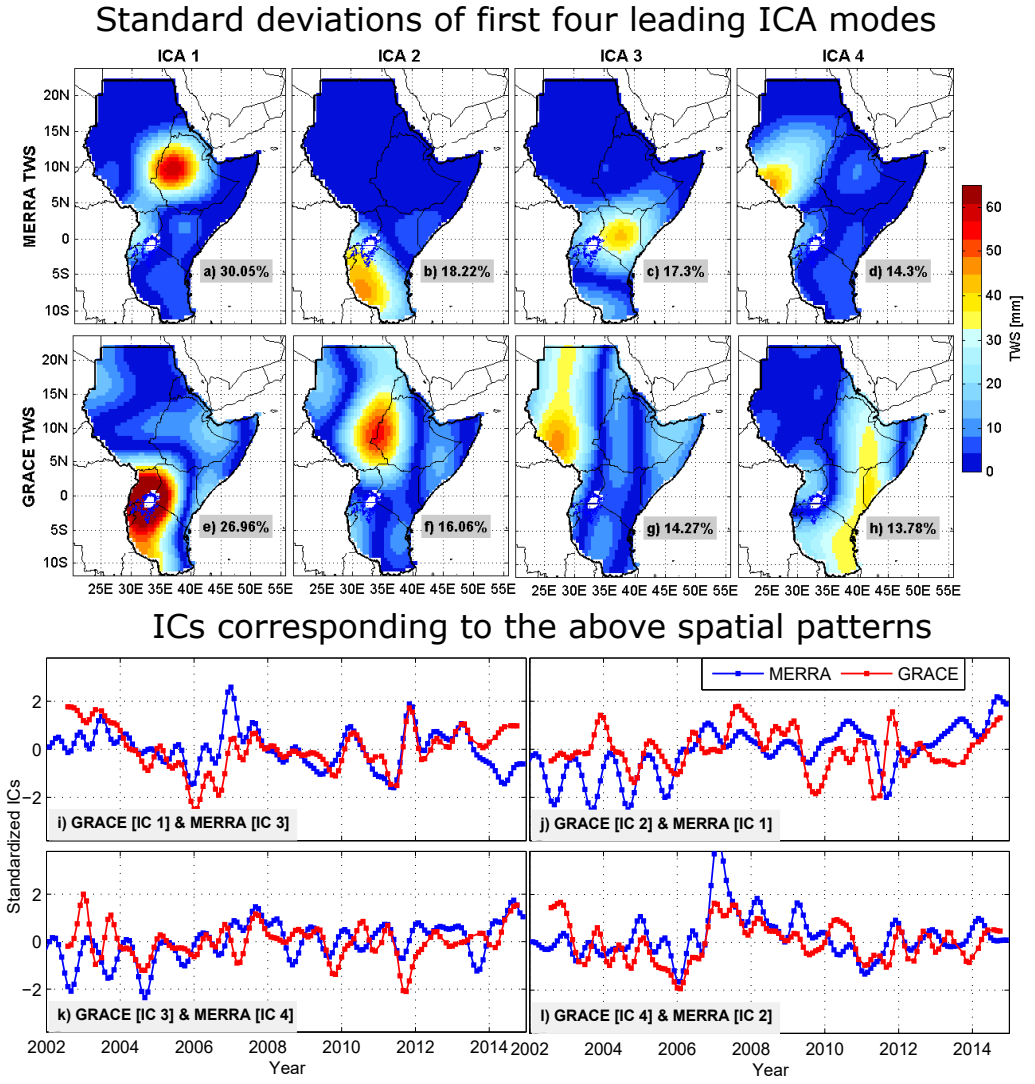

Figure 7: The first four dominant modes of TWS variability over the GHA region based on (a-d) MERRA (1980-2014) and (e-h) GRACE data (2002-2014). The corresponding temporal patterns (or ICs) are shown in the bottom panels (e-h), where a 6-month low-pass filter is applied to enhance their interpretation. (i) Temporal patterns corresponding to c & e, (j) a& f, (k) d & g, and (l) b & h.

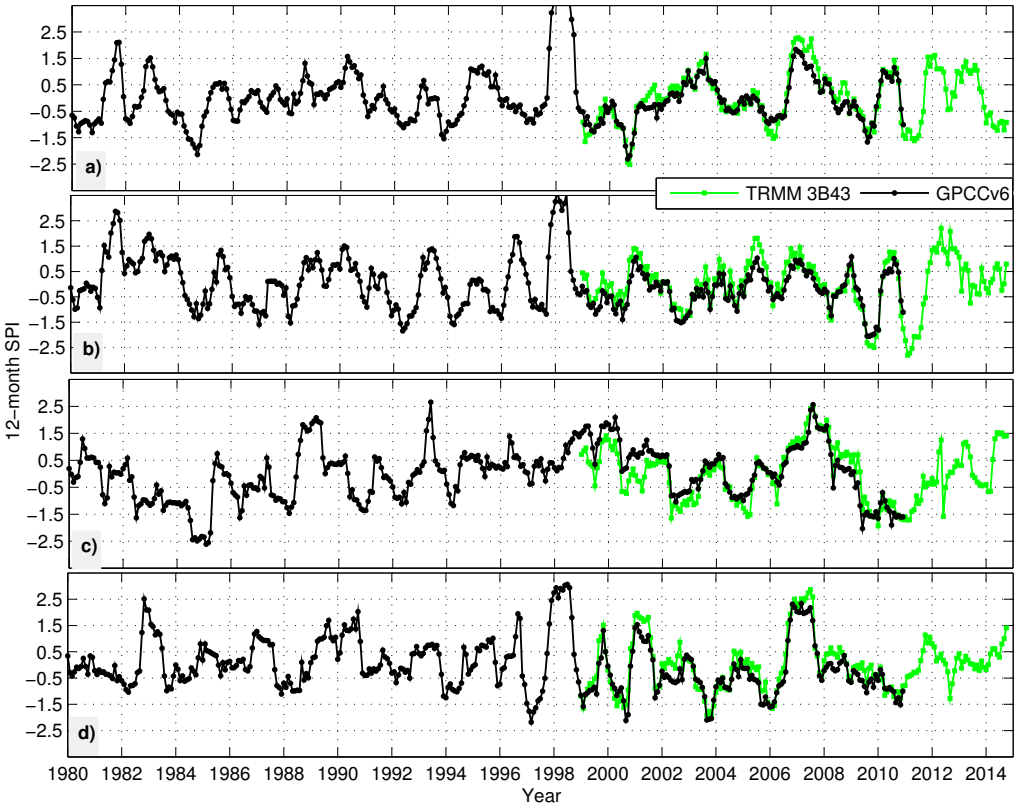

Figure 8: 12-month SPI indices estimated from monthly precipitation products of GPCC (1979-2010) and TRMM (1998-2014) over the four homogenous regions classified based on sICA (see also, Table 3). a) Region 1, b) Region 2, c) Region 3, and d) Region 4. Note that SPI was not calculated for the first 12 months in both datasets.

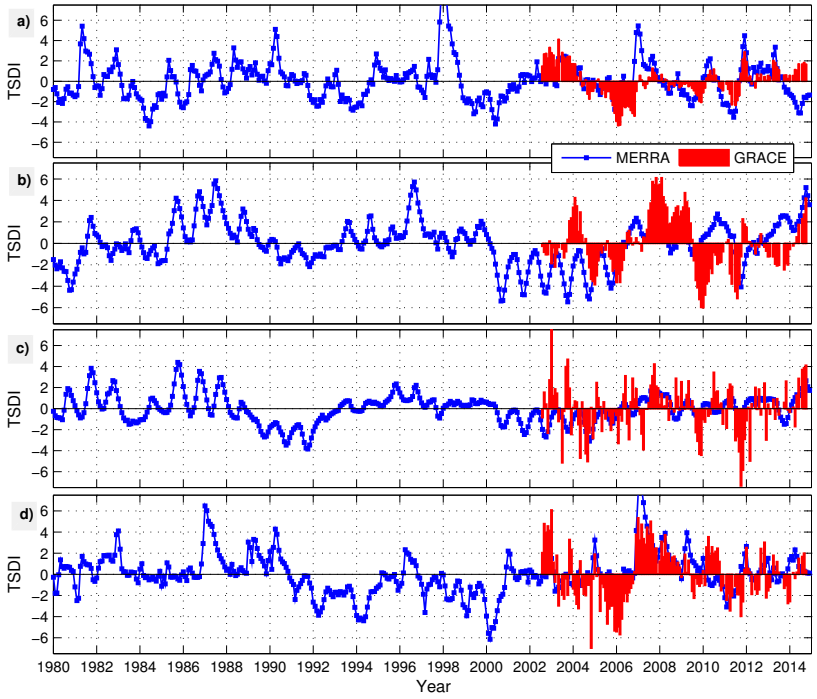

Figure 9: TSDI indices computed based on sICA-derived modes over (a) Region 1, (b) Region 2, (c) Region 3, and (d) Region 4 (see Table 3).

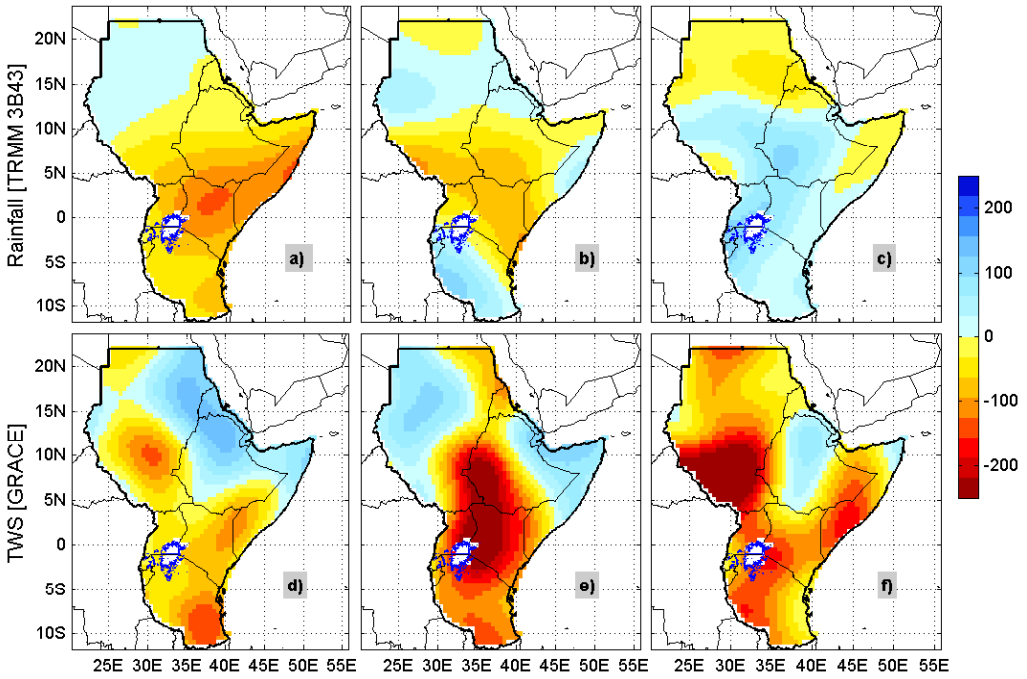

Figure 10: Seasonal rainfall anomaly and TWS changes (mm/season) over the GHA region during a-b) October-December 2010, c-d) March-May 2011, and e-f) June-September 2011.

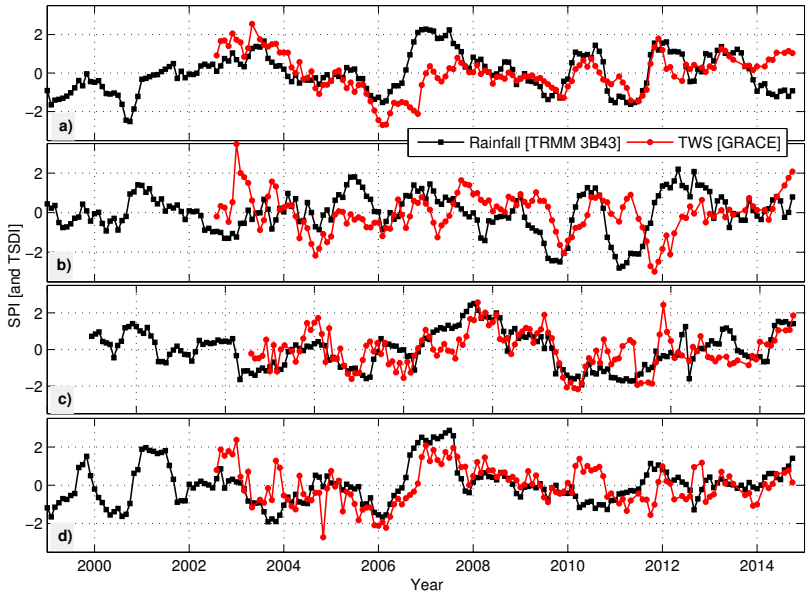

Figure 11: SPI and TSDI indices of TRMM precipitation product and GRACE TWS changes for the period 1999 to 2014. The TSDI indices were normalized to the SPI to highlight their temporal pattern over the four regions.

Table 1: Various categories of droughts and wet conditions based on the SPI Index (McKee et al., 1993; Viste et al., 2013).

SPI	**Category**
+2.0 and above	Extreme wet
+1.5 to +1.99	Very wet
+1.0 to +1.49	Moderately wet
+0.99 to -0.99	Normal
-1.0 to -1.49	Moderate drought
-1.5 to -1.99	Severe drought
-2 and below	Extreme drought

Table 2: Various categories of droughts and wet conditions based on the TSDI Index (Palmer, 1965; Yirdaw et al., 2008).

TSDI	**Category**
+4.0 and above	Extreme wet
+3.0 to +3.99	Very wet
+2.0 to +2.99	Moderate wet
+1.99 to -1.99	Normal
-2.0 to -2.99	Moderate drought
-3.0 to -3.99	Severe drought
-4 and below	Extreme drought

Table 3: Four sub-regions classified according to the first four leading modes of precipitation and TWS.

Region	**Area**	**GPCC v6**	**TRMM 3B43**	**MERRA**	**GRACE**
Region 1	Kenya Uganda Rwanda Burundi Northern Tanzania	ICA1	ICA1	ICA3	ICA1
Region 2	Ethiopia Sudan	ICA2	ICA3	ICA1	ICA2
Region 3	South Sudan	ICA4	ICA4	ICA4	ICA3
Region 4	Tanzania Eastern Ethiopia	ICA3	ICA2	ICA2	ICA4

Table 4: Severe to extreme meteorological droughts based on the SPI in the four regions (see, Table 3) of GHA from 1979 to 2014.

Region	**Periods**	**Duration**	**SPI [Max]**	**Class**
Region 1	Jul 1983-Feb 1985	20 months	-2.13	Extreme
	Apr 1993-Sep 1994	18 months	-1.54	Severe
	Nov 1998-Mar 2002	43 months	-2.31	Extreme
	Mar 2004-Jul 2006	29 months	-1.53	Severe
	Jun 2008-Nov 2009	19 months	-1.66	Severe
	Nov 2010-Sep 2011	12 months	-1.62	Severe
Region 2	Apr 1984-Apr 1985	13 months	-2.13	Extreme
	Jan 1986-Jul 1988	28 months	-1.60	Severe
	Oct 1991-Dec 1992	15 months	-1.84	Severe
	Nov 1993-Nov 1994	13 months	-1.59	Severe
	Apr 2002-Jan 2004	22 months	-1.52	Severe
	Feb 2009-Feb 2010	13 months	-2.50	Extreme
	Oct 2010-Oct 2011	13 months	-2.80	Extreme
Region 3	Jul 1982-Sept 1985	39 months	-2.57	Extreme
	Apr 1982-May 1985	38 months	-2.61	Extreme
	Mar 2009-July 2012	41 months	-2.03	Extreme
Region 4	Dec 1987-Mar 1989	16 months	-1.54	Severe
	Nov 1996-Sep 1997	9 months	-2.18	Extreme
	Nov 1998-Oct 2000	24 months	-2.14	Extreme
	Mar 2003-Jul 2006	41 months	-2.10	Extreme
	Dec 2008-Jul 2011	32 months	-1.52	Severe

Table 5: Severe to extreme hydrological droughts based on the TSDI in the four regions (see Table 3) of GHA derived from MERRA (1980-2014) and GRACE (2002-2014) products.

	MERRA (1980-2014)				GRACE (2002-2014)			
Region	Periods	Duration	TSDI [Max]	Category	Periods	Duration	TSDI [Max]	Category
Region 1	Nov 1983-May 1987	43 months	-4.33	Severe	Sep 2004-Nov 2006	27 months	-4.31	Severe
	Mar 1992-Mar-1996	49 months	-4.05	Extreme	Jun 2008-Feb 2010	21 months	-2.08	Moderate
	Feb 2000-Nov 2002	34 months	-3.34	Severe	Sept 2010-Sep 2011	13 months	-2.58	Moderate
	Oct 2010-May 2012	20 months	-3.68	Severe				
Region 2	Jan 1980-Jul 1981	19 months	-5.02	Extreme	Mar 2004-Nov 2006	33 months	-3.36	Severe
	Apr 2000-Jun 2006	75 months	-6.25	Extreme	Sep 2009-Oct 2011	26 months	4.60	Extreme
	Jul 2011-Jul 2012	13 months	-4.72	Extreme				
Region 3	Dec 1998-Mar 1993	52 months	-5.93	Extreme	May 2004-Nov 2006	31 months	-3.26	Extreme
	Jul 2000-Mar 2002	21 months	-3.9	Severe	Jun 2009-Sep 2011	28 months	-4.40	Extreme
	Jun 2000-Feb 2006	45 months	-4.81	Extreme				
Region 4	Feb 1991-Mar 1996	62 months	-5.84	Extreme	Mar 2004-Oct 2006	32 months	-5.70	Extreme
	Jan 1997-Jan 2001	49 months	-6.93	Extreme	Nov 2011-Jan 2014	27 months	-3.98	Severe
	Nov 2005-Nov 2006	13 months	-3.47	Severe				
	May 2010-Nov 2011	19 months	-3.17	Severe				

Table 6: Correlations between TSDI derived from GRACE TWS changes and SPI derived from TRMM precipitation estimates between 2002 and 2014. Correlations between GRACE and MERRA TSDIs are also shown to indicate the skills of MERRA with respect to TWS changes derived from GRACE observations. Correlation coefficients that are significant at 95% confidence level are indicated in bold.

Region	**Region 1**	**Region 2**	**Region 3**	**Region 4**
SPI and TSDI (GRACE)	**0.44**(1 month)	0.24 (2 month)	**0.52** (3 month)	**0.59** (1 month)
MERRA vs GRACE (TSDI)	**0.47**(1 month)	**0.51**(0 month)	**0.46**(1 month)	**0.57**(0 month)

Table 7: Correlations (significant at 95% confidence level) and lags (in brackets) between rainfall (and TWS) and ENSO/IOD between 1979-2014. Negative months' lags indicate ENSO/IOD occurs before rainfall or variations of TWS and vice versa. Correlation coefficients that are significant at 95% confidence level are indicated in bold.

Region	**Products**	**ENSO (Niño3.4)**	**IOD (DMI)**
Region 1	GPCC v6 (1979-2010)	**0.33** (-1)	**0.48** (-1)
	TRMM 3B43 (1998-2014)	**0.44** (-1)	**0.53** (-1)
	MERRA (1980-2014)	-0.23 (5)	-0.18 (6)
	GRACE (2002-2014)	**0.38** (-6)	**-0.42** (-6)
Region 2	GPCC v6 (1979-2010)	**0.44** (-1)	**0.53** (-1)
	TRMM 3B43 (1998-2014)	-0.26 (-6)	-0.07 (-2)
	MERRA (1980-2014)	-0.26 (1)	-0.24 (1)
	GRACE (2002-2014)	**0.48** (-1)	**0.57** (-5)
Region 3	GPCC v6 (1979-2010)	-0.23 (1)	-0.18 (-6)
	TRMM 3B43 (1998-2014)	-0.26 (-1)	-0.20 (-1)
	MERRA (1980-2014)	**-0.37** (3)	**-0.44** (3)
	GRACE (2002-2014)	-0.21 (2)	**-0.34** (-6)
Region 4	GPCC v6 (1979-2010)	-0.23 (-1)	**0.39** (-2)
	TRMM 3B43 (1998-2014)	-0.20 (-6)	**0.34** (-1)
	MERRA (1980-2014)	-0.22 (7)	**-0.34** (6)
	GRACE (2002-2014)	**0.34** (-6)	**0.41** (-6)